MESOSCALE ANALYSIS OF MULTI-SPAN MASONRY ARCH BRIDGES

E. Tubaldi [1,2*], E. Minga[1], L. Macorini[1], and B.A. Izzuddin[1]

[1] Department of Civil and Environmental Engineering, Imperial College London, South Kensington Campus, London, UK

[2] Department of Civil and Environmental Engineering, University of Strathclyde, Glasgow, UK, ([*]corresponding author)

Keywords: Masonry arch bridges, Multi-span, Mesoscale model, Backfill.

Abstract. Masonry arch bridges often include multiple spans, where adjacent arches and piers interact with each other giving rise to a complex response under traffic loading. Thus, the assumption commonly used in practical assessment that multi-span masonry viaducts behave as a series of independent single-span structures, may not be realistic for many configurations. While several experimental and numerical studies have been conducted to investigate single-span masonry arches and bridges, only limited research has been devoted to the analysis of the response of multi-span masonry bridges. This study investigates numerically masonry arch bridges with multiple spans subjected to vertical loading. For this purpose, an advanced finite element description, which is based upon a mesoscale representation for masonry and accounts for both material and geometric nonlinearities, is employed to shed some light on the actual behaviour of these structural systems. A validation study is first carried out to confirm that the adopted modelling strategy is capable to accurately simulate previous experimental results. Then, the influence of some critical geometrical and mechanical parameters that affect the bridge response is evaluated through a parametric study. The effects of pier settlements and brickwork defects are also investigated, as well as the interaction between adjacent spans through comparisons against the response of single-span counterparts.

1 INTRODUCTION

Masonry arch bridges are heterogeneous systems consisting of multiple components, such as the arch barrel, the backfill, the lateral walls, the piers and the abutments [1], which mutually interact giving rise to a complex response under traffic loading. These mostly old bridges have proven to be very resilient and enduring structures, which still constitute a significant portion of the bridge stock in many nations. For this reason, the accurate prediction of their load capacity against traffic and extreme loadings (e.g. floods) is a task of extreme importance, which calls for the use of advanced models providing accurate predictions of their complex nonlinear response [2-7].

In the last few decades, numerous experimental and numerical studies were carried out on masonry arch bridges, as recently documented in [6, 8]. However, there are still many open issues that need to be addressed. First of all, to date the focus of most experimental and numerical research efforts was on single span masonry arches, whereas multi-span bridges have received less attention and many studies have focused on other types of actions such as seismic [9] or scouring [10]. However, assuming that multi-span bridges behave as a series of separate single-span structures may be not realistic even under vertical loads acting on a single span. This is because adjacent spans interact with each other and with the substructures, potentially leading to a reduced capacity against vertical loads.

Some geometrical parameters such as the pier slenderness, the rise-to-span ratio, the loading position, and the pier height may affect significantly the behaviour up to collapse. This problem has been investigated only by a few studies, based often on simplified models. For example, Hughes [11] employed a simple mechanism approach to analyse twin-span bridges and evaluate the effect of different geometrical parameters and the reduction of the ultimate capacity with respect to single-span arch structures. Cavicchi and Gambarotta [12] employed a two-dimensional finite-element limit-analysis procedure to investigate the complex interaction between piers, arches and fill at collapse. The fill was described using triangular elements connected by interface elements, neglecting dilatancy effects. Brencich and De Francesco [13] studied the influence of some geometrical parameters, such as the pier slenderness, the rise-to-span ratio, the loading position, and the pier height on the collapse behaviour of multi-span bridges through a one-dimensional elasto-plastic representation of the piers and the arches. The contributions of the spandrel walls and the arch barrel–fill interaction were also neglected. De Felice [14] analysed the load capacity of multi-span masonry arch bridges using fibre beam elements for modelling the masonry components, and a simplistic approach with non-linear horizontal trusses carrying compression only to represent the interaction with the backfill. The results of this study pointed out that the assumption of infinite ductility, which is at the base limit analysis, generally yields unconservative predictions. Oliveira et al. [15] used a rigid block limit analysis approach [16] to analyse the influence of geometrical and mechanical characteristics on the ultimate response of multi-span bridges in the northwest Iberian Peninsula. This study showed that multi-span bridges with deep arches exhibit a behaviour similar to single-span structures, while those with semi-shallow arches have a lower capacity compared to the same bridges with single span. In these numerical simulations, the assumption of zero tensile resistance of the mortar joints was made, and simplified representations of the backfill and of the arch barrel–backfill physical interface were used, which may lead to inaccurate response predictions. Altunışık et al. [17] focused on the thickness of the arch and how increasing it results in a decrease of maximum displacements, tensile stresses and strains, and in an increase of compressive stress and strains.

Thus, based on a review of the existing literature, it can be confirmed that there is a need of more accurate models to i) identify the critical geometrical and mechanical parameters controlling the capacity of multi-span masonry bridges and ii) understand their effect on the bridge behaviour under service and collapse loads.

The authors of this study have developed in previous works an advanced approach for investigating the behaviour of masonry arches [4-5] and single-span masonry arch bridges [18-20] subjected to vertical loading, as well as to the effects of scour at the base of the piers [21]. This approach is based on a meso-scale description of masonry arches and piers, and accounts for both material and geometric nonlinearities of the various bridge components. The authors have recently presented some preliminary results obtained by applying this detailed modelling strategy to the analysis of multi-span masonry bridges under vertical loading [22]. This paper extends this early attempt by providing a comprehensive numerical investigation. In particular, in the first part of the paper a model validation study is carried out, considering the tests carried out in the past at the Bolton Institute [23], where a three-span masonry arch bridge with detached spandrel walls was loaded to collapse. The numerical simulation of the tests is based on a strip model of the tested bridge, providing a simplified but accurate description of the problem. Subsequently, the response of the numerical model is studied under the effect of settlements, and a parametric analysis is carried out to investigate how various geometrical and mechanical parameters affect the structural behaviour up to collapse. The critical role of the interaction between adjacent spans is investigated by means of comparisons with the case of single-span arches.

2 MODEL DESCRIPTION

Masonry is a composite material, whose nonlinear non-isotropic behaviour depends on the type of masonry bond as well as on the direction of loading, and in which the mortar joints often represent the weakest component [24]. These specific features must be taken into account in developing an accurate mechanical representation of arches and piers in masonry bridges.

While it is still possible to employ continuous approaches for describing masonry as an equivalent homogeneous material [25], a mesoscale modelling strategy is employed here for the piers and the arches. This approach, implemented in standard FE procedures and accounting for both mechanical and geometrical nonlinearities, allows to accurately describe the 3D domain of the masonry components, with the 3D masonry bond explicitly represented using two or more elastic 20-noded solid elements for each brick, and 2D 16 nodes nonlinear interface elements with zero-thickness for the mortar joints [19,26]. In this way, it is possible to describe the typical fracture modes that characterise the nonlinear response of masonry arches up to collapse. These include flexural cracking, frictional sliding and masonry crushing. The formation of radial cracks and circumferential cracks in the mortar joints, leading to ring separation in the case of multi-ring arches, can be simulated. A recently developed cohesive-frictional constitutive model [27] is employed for the interface elements, providing computationally robust and efficient solutions of the local equilibrium problem. Geometric nonlinearity is described by using a corotational formulation.

An accurate prediction of the response of masonry arch bridges requires a realistic representation of the behaviour of the fill and of its interaction with the arch barrel. In the proposed modelling strategy, the backfill domain is described through a continuous approach, and employing a mesh of 15-noded elasto-plastic tetrahedral elements with an elasto-plastic material behaviour. A similar approach was followed in other studies on masonry arch bridges (see e.g. [25]). The isotropic elastic response is characterized in terms of Young's modulus and Poisson's ratio, whereas the plastic behaviour is described through a modified Drucker-Prager (D-

P) yield criterion, with a tension and compressive caps as in [21] (see also [28,29]). In order to avoid excessive dilatancy effects, a non-associative flow rule is adopted. It is noteworthy that the D-P yield envelope is essentially a smooth approximation of the Mohr–Coulomb yield surface, and therefore its parameters can be expressed as functions of the cohesion c and the friction angle ϕ. In particular, the D-P yield envelope passes through the inner edges of the Mohr–Coulomb yield surface [21].

In order to improve the efficiency of the computational strategy, a mortar mesh tying method is used. This method allows to mesh independently the non-conforming interfaces of the backfill and the arch barrel domains. Thus, the two domains can also be meshed separately by optimizing the mesh size and shape [18]. Zero-thickness interface elements with nonlinear behaviour are used to describe the interaction between the arch and the backfill, allowing for separation and frictional sliding. Finally, the use of a partitioned modelling strategy [30-32] allows to further enhance the computational efficiency. This is of extreme importance for the analysis of multi-span masonry arch bridges, which are large structures whose analysis would require excessive computational demand using standard monolithic simulations.

3 MODEL VALIDATION

The modelling strategy described in the previous section is validated by considering the tests carried out at the Bolton Institute (UK) on a three-span masonry arch bridge prototype, Bridge no.2 [23]. The spandrel walls of this prototype are detached from the arch barrel, and provide only a transverse restraint to the backfill, without interacting with the arch and not contributing to the global stiffness and resistance. The two-ring arch barrels are built with a stretcher method in a segmental circular shape. The arches are 215 mm thick, with a 4:1 span-to-rise ratio and a springing angle of 37°. English bond brick-masonry is used for the spandrel and wing walls. The brickwork consists of full size Class A engineering bricks and a 1:2:9 (cement:lime:sand) mortar, while the space above the arch and between the two lateral walls (spandrel and wing walls) is filled with 50 mm graded crushed limestone. The geometrical properties of the main bridge components are summarized in Table 1.

In the test, a steel loading beam of dimensions 2600×420 mm^2 was placed on the top surface of the backfill and used to apply a vertical line load at a quarter of the central span. The beam was pushed against a reaction frame anchored in the base slab. The line load was uniformly distributed along the full width of the backfill and was progressively increased up to bridge collapse, which occurred due to seven large radial cracks (hinges) forming in the mortar radial joints of the arch as well as at the extremes of the right pier.

Table 1: Dimensions of the bridge components.

Arch	**Span *s* (mm)**	**Rise *r* (mm)**	**Ring thickness *d* (mm)**	**Width (mm)**	**n. of bricks**
	3000	750	215	2880	48
Backfill	**Depth at crown *f* (mm)**		**Width (mm)**	**Length (mm)**	
	300		2880	2460×2+3000	
Spandrel walls	**Depth at crown (mm)**		**Width (mm)**	**Length (mm)**	
	300		330	2460×2+3000	
Piers	**Height *h* (mm)**		**Thickness (mm)**	**Width *w* (mm)**	
	1500		2880	440	

A reduced representation of the bridge is developed in ADAPTIC [33], using a strip model with only one set of solid elements along the bridge width for both the arch and the backfill meshes. The transverse confinement to the backfill provided by the rigid spandrel walls, detached from the arch barrel, is described by appropriate boundary conditions, i.e., by restraining the displacements of the nodes belonging to the outer faces of the backfill and the arch along the direction *z* (Figure 1). It is noteworthy that this efficient representation was shown to yield accurate results in the case of masonry arches and single-span bridges under the action of line loads uniformly distributed along the width of the arch structures [4,19].

Figure 1 illustrates the proposed simplified FE model of the bridge, using a mesoscale approach for describing the actual masonry bond of the arches and piers. In particular, the radial mortar joints between the bricks in the arch barrel are described via two nonlinear interface elements. For each arch, 96 20-noded elastic solid elements describe the brick units, 94 nonlinear interface elements the mortar bed joints, 48 nonlinear interface elements the circumferential mortar joints connecting the adjacent rings, and 48 interface elements the interaction between the arch and the fill.

The backfill mesh consists of 15-noded tetrahedral elements, with mesh refinement at the abutments and close to the loading area at the quarter span, for a total of 135 15-noded elements for each span. A mesh tying approach [18] is used to link the non-conforming sides of the contact interface simulating the interaction between the infill and the arch. The wedged skewback stones at the top of the piers are discretised using 15-noded tetrahedral elements, which are assigned the same properties as the brick elements. Additional mortar interfaces are considered at the boundary of the skewback, to allow for formation of further cracks between the skewback and the pier or the arches.

Fixed supports are considered at the two bases of the backfill domain corresponding to the abutments, whereas the two vertical faces of the backfill are restrained longitudinally (along *x* in Figure 1). In order to prevent transverse deformations within the bridge, the two longitudinal outer faces of the strip model of the bridge (at z=0mm and z=240mm) are restrained along *z*, corresponding to a 2D plain-strain modelling approach.

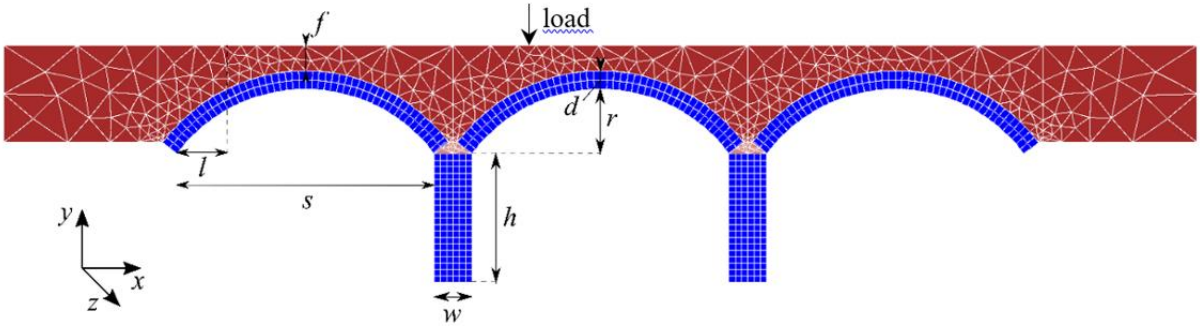


Figure 1. FE mesh of analysed bridge model and geometric parameters.

It is noteworthy that many key parameters of the model have been directly measured or have been identified from experimental test results, including material densities, backfill cohesion and friction angle properties, brickwork elasticity modulus and compressive and shear bond strength. The self-weight of the bridge components is taken into account assuming unit weights ρ_m = 22.7 kN/m^3 and ρ_f= 22.2 kN/m^3 for masonry and the fill, respectively. The masonry units are assumed to have a linear elastic behaviour, characterized by a Young's modulus E_b =35000 MPa and a Poisson's ratio v_b = 0.15. The values of the normal and tangential stiffness of the mortar interfaces are respectively K_n = 400 N/mm^3 and K_v = 167 N/mm^3. The assumed properties of the solid elements and of the interfaces correspond to an equivalent homogenised value

of the elasticity modulus of the brickwork of 16000 MPa, evaluated by employing the approach of Pande [34]. This corresponds to the average of the values according to the compressive tests carried out on small brickwork specimen in both [23] and [35].

The values of the cohesion c, tensile strength f_t, friction angle $tan\phi$, and compressive strength f_c, reported in Table 2, define the multi-surface plasticity criterion of the coupled damage-plasticity model used for the cohesive interfaces according to [27]. An anisotropic damage tensor describes the effects of strength and stiffness degradation. The variables describing the evolution of damage develop with the evolution of the plastic work. The three values of the fracture energy reported in Table 2 refer to the failure under tensile stresses ($G_{f,1}$), shear stresses ($G_{f,2}$), and compressive stresses ($G_{f,3}$) and define the point of complete damage in the respective modes.

The backfill domain, consisting of crushed limestone material, is modelled utilising a modified DP criterion fitted to the MC inner edges, with Young's modulus E_f =50 MPa, Poisson's ratio v_f= 0.20, cohesion c_f = 0.001 MPa (a zero value would lead to numerical issues), friction angle φ_f = 55°, and dilatancy angle φ_d = 25°. The values of c_f and φ_f are based on shear box tests.

Finally, the interface elements representing the physical interface between the arch and backfill have negligible cohesion and tensile strength and a friction angle of 60°, which does not degrade because of damage. The parameters of the mesoscale model for brick-masonry and of the elasto-plastic model for the backfill have the same values as those used in previous numerical studies [27], where the tests on single-span arch bridge models carried out at Bolton Institute [35] were simulated. The only exception is the value of the Young's modulus of the backfill material, which is equal to E_f =50 MPa instead of the value E_f =200 MPa considered in [18]. The adopted value of E_f leads to a better match with the experimental tests, and is consistent with a lower level of compaction of the backfill achieved in the case of multi-span bridges, as reported in [23].

To improve computational efficiency in the nonlinear analysis of the bridge model, which has overall more than 35000 degrees of freedom, the domain partitioning approach [30-32] is used, with 22 partitions that allow for parallel computation in ADAPTIC [33].

Table 2: Mortar joints properties.

Cohesion c [N/mm^2]	**Tensile strength f_t [N/mm^2]**	**Friction angle $tan\phi$**	**Compressive strength f_c [N/mm^2]**	**Fracture energy for each mode**		
				$G_{f,1}$ [N/mm]	**$G_{f,2}$ [N/mm]**	**$G_{f,3}$ [N/mm]**
0.29	0.20	0.50	16.00	0.05	0.05	1.00

Figure 2 shows the collapse mechanism of the numerical model of the bridge, corresponding to the last step of the analysis. This mechanism involves only the central and right span, with significant outward movement of the right pier. Seven wide cracks can be identified in the arch barrels, whose location is in very good agreement with the experimental results.

Figure 3 shows the applied load vs. the vertical displacement of the node on the arch intrados at the quarter span, according to the numerical strip model and the experimental test. The simulated response is quite close to the experimental one, with good agreement in terms of initial stiffness, load capacity and post-peak response.

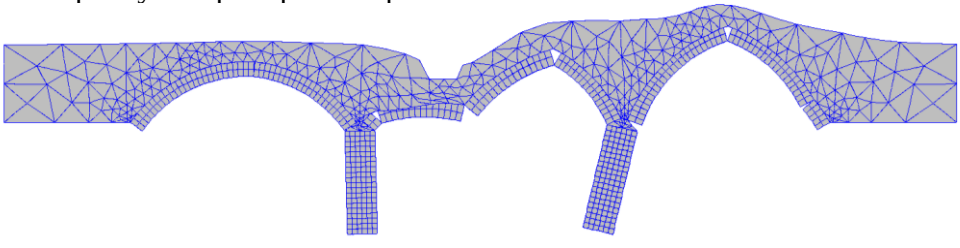


Figure 2. Deformed shape and cracking mechanism at the last step of the analysis.

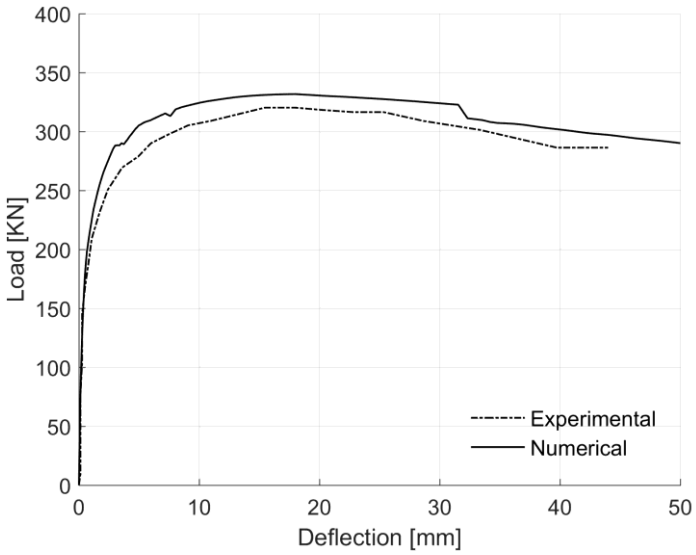
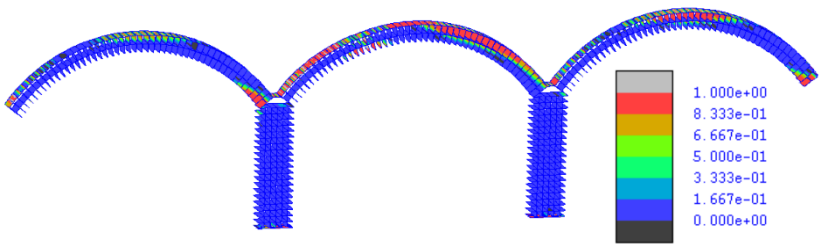


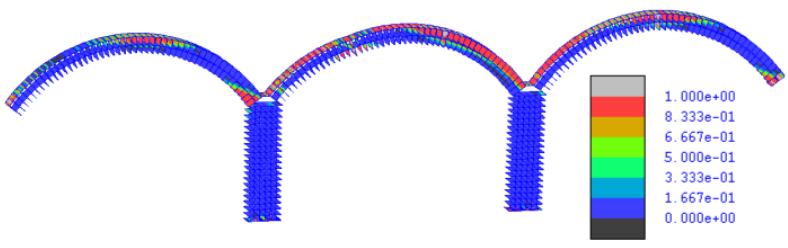
Figure 3. Comparison between experimental and numerical results in terms of applied force vs. displacement at a quarter of the central span.

Figure 4 shows the values of the damage parameter in tension of the interfaces for increasing load levels, describing the evolution of the cracks in the arch barrel and of the damage at the arch-fill interface. It can be observed that only for high levels of the loading, the damage involves also the interfaces of the first span, although major cracks cannot be visualised in Figure 2. In addition to the damage observed in the plastic hinges forming in the arch and the piers, significant damage can be noted at the top circumferential interface between the arch and the backfill, particularly in correspondence of the central span.

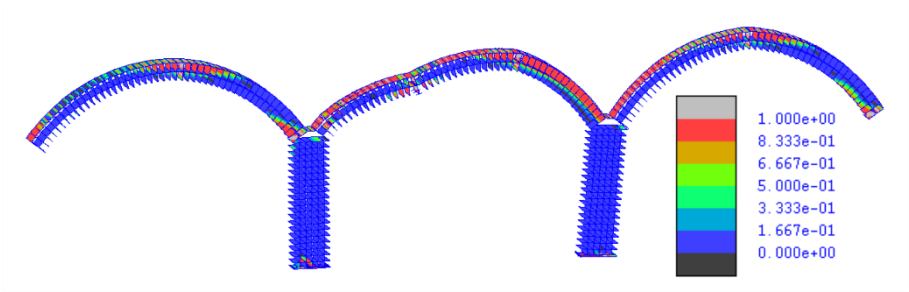
a)



b)



c)



d)

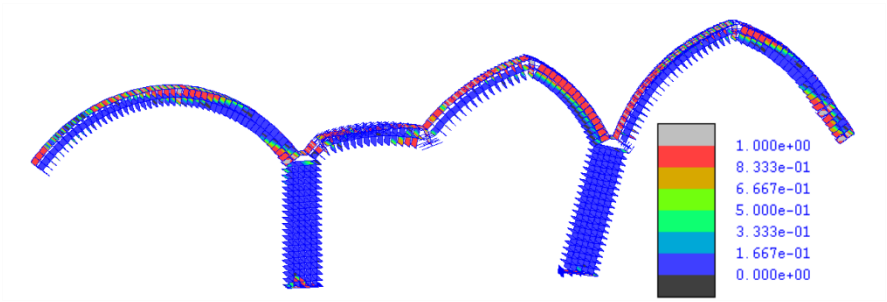
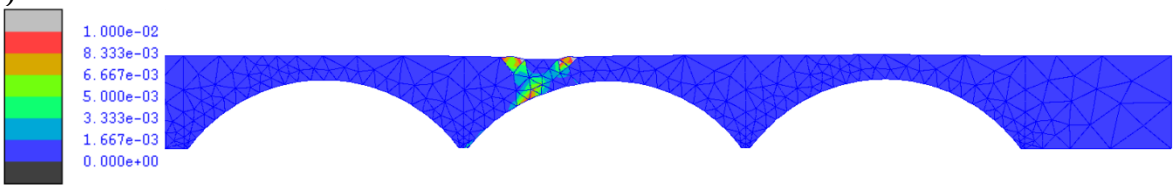


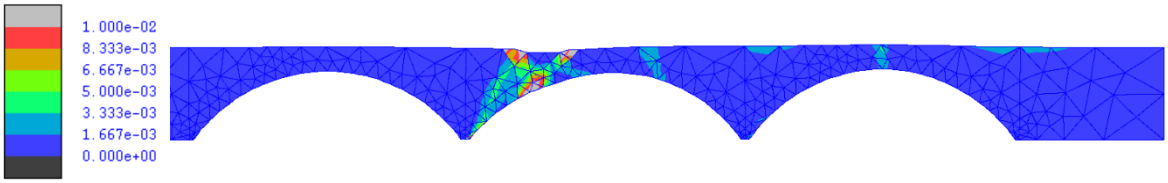
Figure 4. Evolution of the damage parameter in tension of the interfaces: (a) P = 282.22 kN, (b) P = 305.98 kN, (c) P = 331.76 kN, (d) P = 270.52 kN (final step of analysis).

The evolution of the inelastic behaviour of the backfill is described by the von Mises plastic deformations, shown in Figure 5 for increasing loading levels. These plastic deformations occur first in the central span, below the loading area, and then they develop at the first quarter of the central span and at the third quarter as the load increases. In the final stages of the loading history, plastic deformations can be observed also in the third span, whereas the backfill in the first span behaves elastically, consistently with the plastic mechanism observed in Figure 2 and involving only the second and third span.

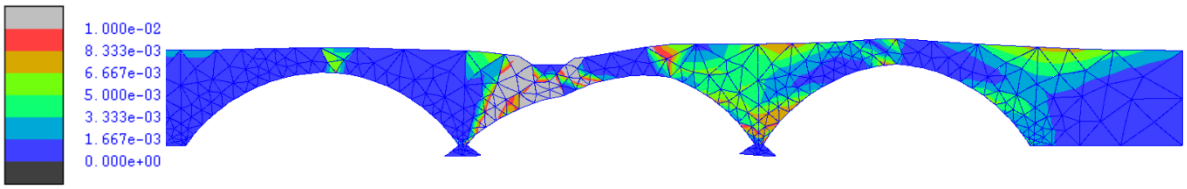
a)



b)



c)



d)

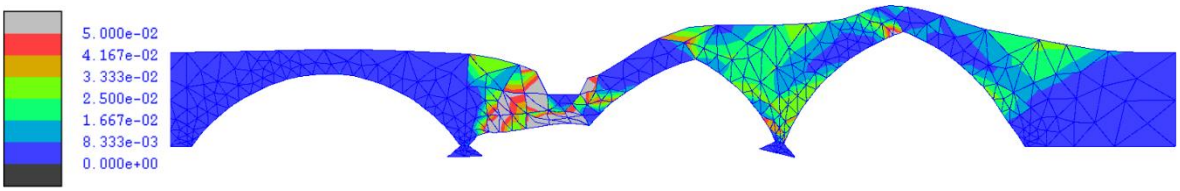


Figure 5. Evolution of the equivalent Von Mises plastic deformations in the backfill: (a) P = 282.22 kN, (b) P = 305.98 kN, (c) P = 331.76 kN, (d) P = 270.52 kN (final step of analysis).

4 PARAMETRIC STUDY

This section presents and discusses the results of a parametric study carried out to investigate the effects of settlements, and of several geometrical and mechanical parameters of the bridge model developed in the previous section.

4.1 lnfluence of settlements and rotational stiffness at the piers' foundations

Differential vertical settlements at the bases of the piers and abutments are often responsible for deterioration and reduced capacity in masonry arch bridges [38]. To evaluate the influence of these settlements on the behaviour of the bridge up to collapse, the model described in the previous section has been subjected to increasing vertical load after applying different initial vertical displacements at the base of the left pier. Three different displacement values are considered, namely δ_{vs} = 2.5mm, δ_{vs} = 5mm, and δ_{vs} = 10mm.

Figure 6 shows the collapse mechanism of the bridge after application of these settlements. It can be observed that only for δ_{vs} = 10mm there are some notable differences in the collapse behaviour compared to the case of the reference bridge model, with larger cracks opening between the first span and the top of the left pier.

Figure **7** shows the force-displacement curve corresponding to the different initial settlements considered. For low settlement values, the curves are very similar to the one of the reference bridge model, whereas for δ_{vs} = 10mm, both the global stiffness and the vertical load-carrying capacity of the bridge are reduced.

a)

b)

c)

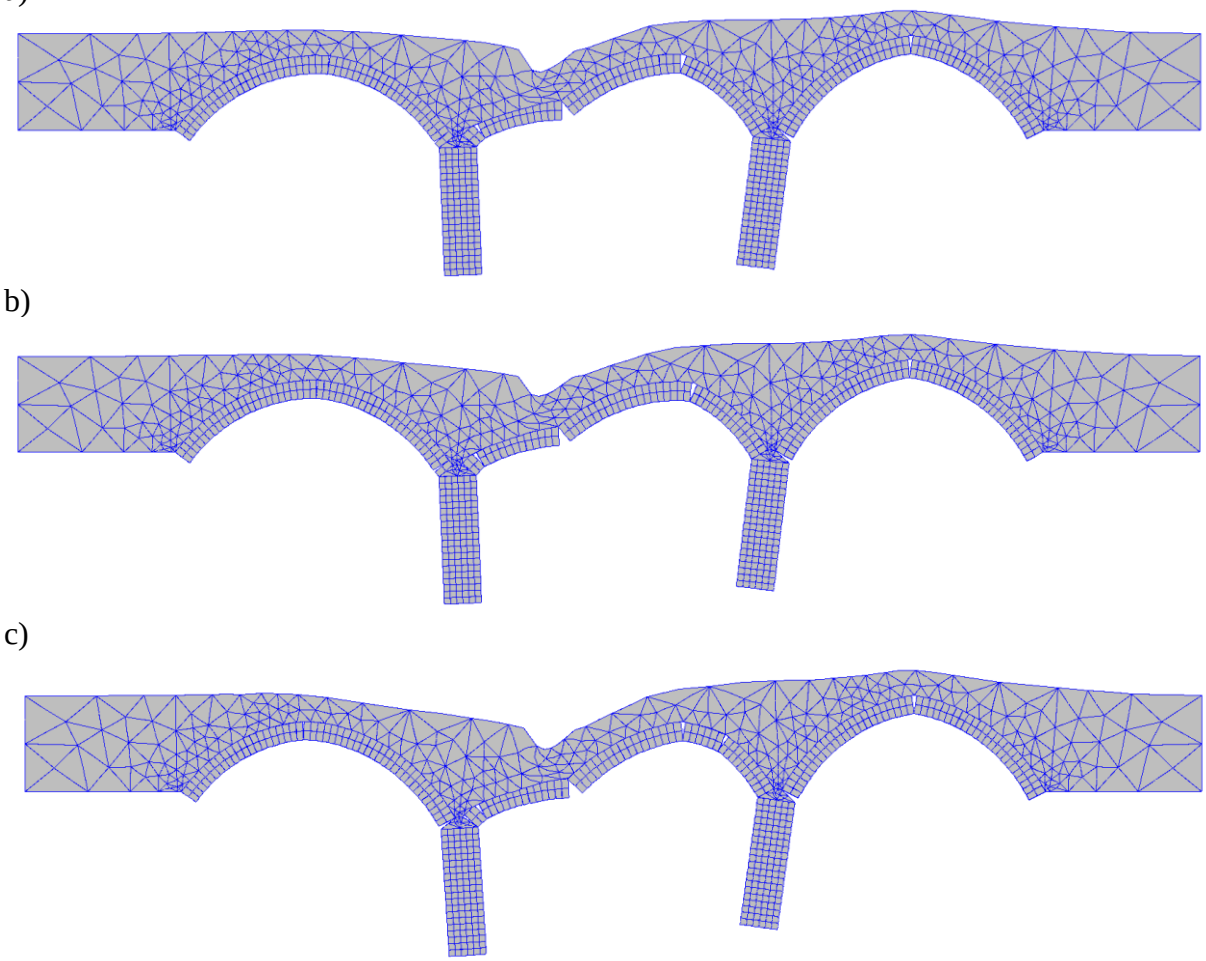


Figure 6. Deformed shape and cracking mechanisms at the final step of the analysis for different values of the initial pier settlement: a) 2.5mm, b) 5mm, c) 10mm (scale = 30).

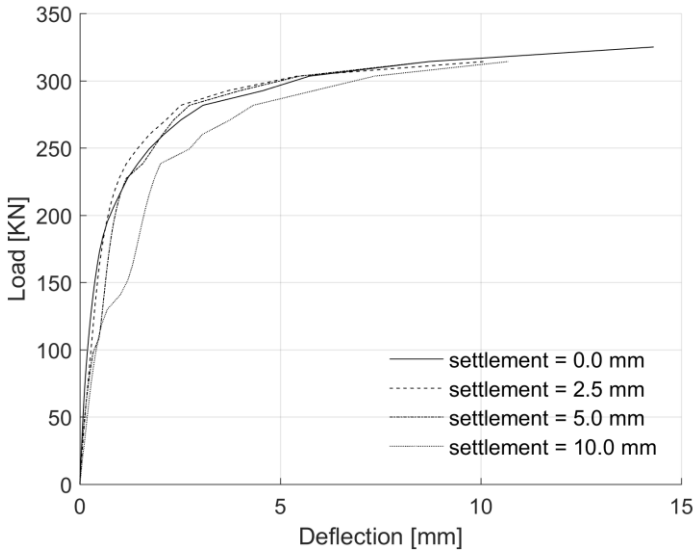


Figure 7. Global response of 3-span bridge for different levels of the initial settlement at the base of the left pier.

Additional numerical simulations have been carried out to investigate the influence of different support conditions at the bases of the two piers. Three different models have been developed

assuming pinned base at the left pier, at the right piers and for both piers. The numerical load-displacement curves are shown in Figure 8, where the load applied at the quarter of the middle span is plotted against the vertical displacement at the masonry arch beneath the loading area. In the figure, the three numerical curves with different support conditions are compared together with the response of the reference model previously validated against experimental data which is characterized by piers with fixed bases. It is found that the support conditions at the pier bases significantly influence the load capacity of the three-span bridge, where an ultimate load reduction of about 19% and 22% is predicted by the models with pinned base at either or both piers.

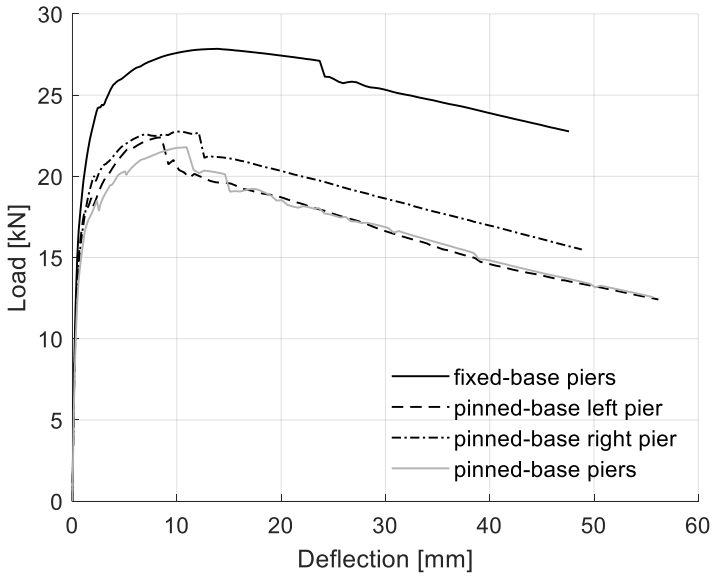


Figure 8. Global response of 3-span bridge for different support conditions at the bases of the two piers.

a)

b)

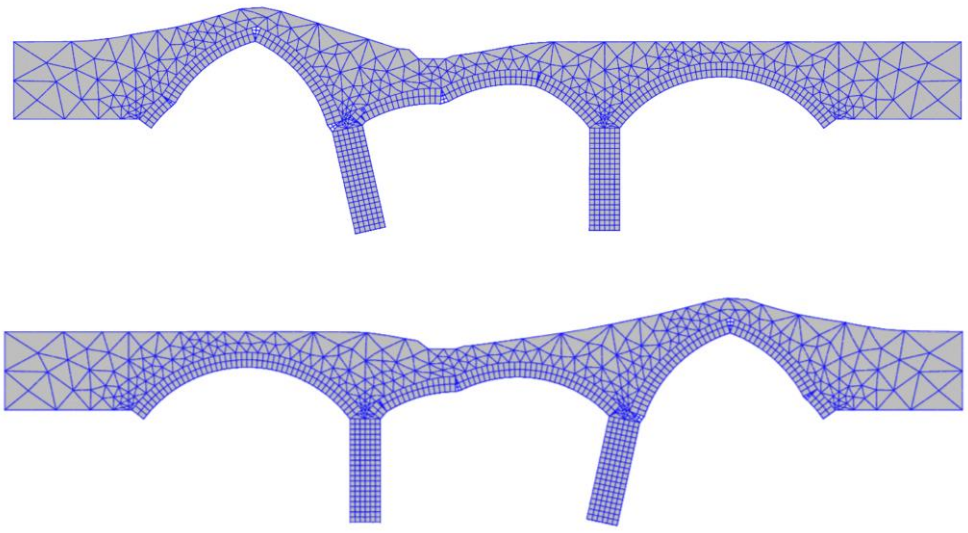


Figure 9. Deformed shape and cracking mechanisms at the final step of the analysis for different pier support conditions: a) pinned base at the left pier, b) pinned base at the right pier (scale = 5).

Different failure mechanisms and cracking patterns in the brickwork are obtained in the three cases. More specifically, the failure mode of the models with pinned bases at the left pier or at both pier bases is characterized by significant damage in the middle and left span with notable

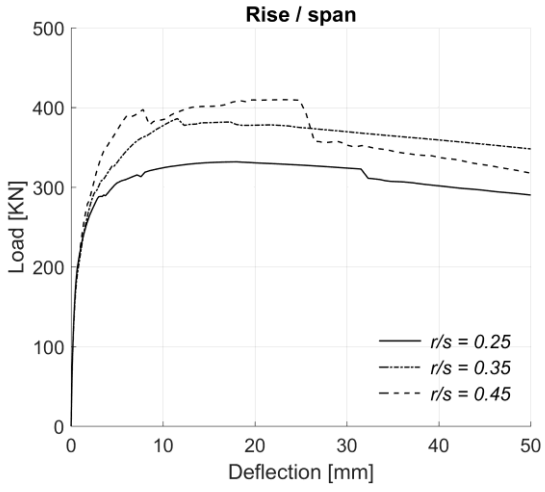
uplift of the latter (Figure 9a). Conversely as shown in Figure 9b, the model with pinned base at the right pier shows a failure mode where damage develops at the middle and the right span, which experiences remarkable cracking and upward displacements at the crown.

4.2 Influence of geometrical parameters

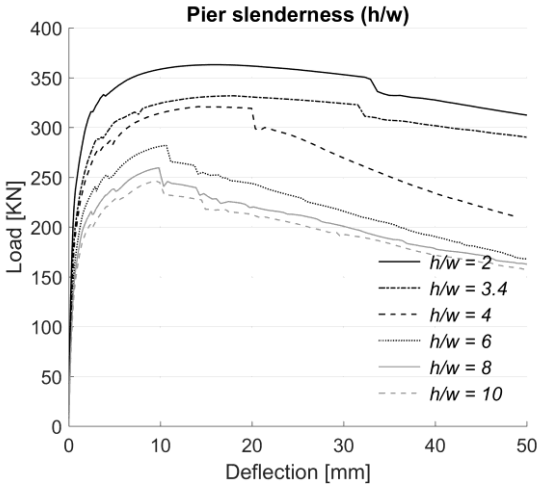
The following parameters are considered to study the influence of the geometrical parameters on the bridge capacity: the rise-to-span ratio (r/s), the pier slenderness (h/w), the location of the vertical load normalized with respect to the span length (l/s), the backfill depth to arch thickness ratio (f/d), and the arch thickness to span ratio (d/s). The investigation is carried out by considering the model described in Section 3 as the reference model, and introducing a variation of each geometrical parameter at a time. The range of variation of the parameters is chosen mainly based on statistical surveys of existing bridges, whose results have been reported in [36-37] and on previous works on the same topic [11].

Figure 10a shows the global force-displacement response of the bridge for different values of the rise-to-span ratio (r/s). Low values of r/s correspond to shallow arches, whereas high values to deep arches. In general, increasing r/s results in an increase of the collapse load, while the initial stiffness does not change significantly. The difference in the load capacity is due to the fact that for a given value of the vertical load, the outward thrust that needs to be counteracted by the piers is higher for shallow arches than for deep arches. This results in high values of the lateral displacement at the top of the relative slender piers in the case of the shallow arch model, which reduces the collapse capacity. Figure 11 shows the collapse mechanism of the bridge model with deep arch (r/s=0.45). Comparing this mechanism to the one of the model with shallow arch (Figure 2), it can be observed that the location of some hinges is shifted upwards. Figure 10b shows the global force-displacement curve of the bridge for different values of the pier slenderness h/w. In general, both the initial stiffness and the collapse capacity reduce for increasing values of the pier slenderness, and the post-peak branch of the curve also becomes steeper. This is because the overturning effect of the thrust transmitted from the arch to the adjacent piers increases for increasing h/w values. It is also worth noting in Figure 12 how the pier slenderness remarkably affects the collapse mechanism: in the case of stocky piers, this mechanism is the same as that of the reference model (Figure 2), whereas in the case of slender piers, it involves the loaded and the first spans, but not the third span.

a)



b)



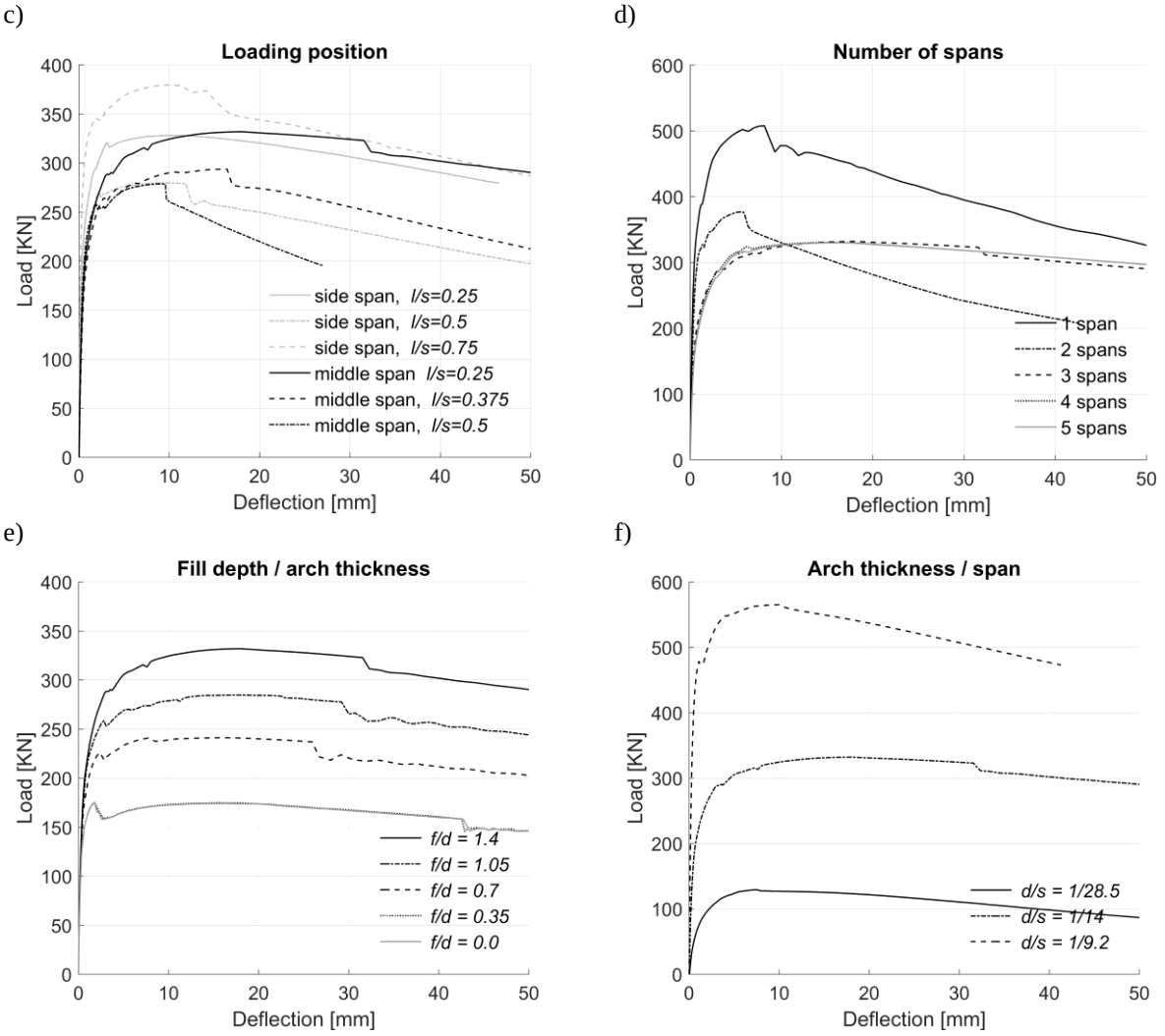


Figure 10. Global response of 3-span bridge for different combinations of the non-dimensional geometrical parameters.

Figure 10c illustrates the influence of the location of the vertical load on the bridge capacity and collapse mechanism. The highest capacity corresponds to a load located at 3/4 of any of the two side spans, whereas the lowest is found for a load located at the middle of the central span. Figure 13 displays the deformed shapes obtained at the end of the numerical simulations for different loading positions on the right-side span. They represent different failure modes and cracking patterns in the brickwork of the first two spans, with the left-side span remaining undamaged in all cases. When the load moves from a position nearer the abutment (l/s=0.25) to the right pier (l/s=0.75), the rotation at the right pier base due to flexural cracking increases leading to a larger uplift movement at the crown of the middle span. This corresponds to a more substantial damage in the arch barrel of the middle span with notable radial cracks forming at the crown, at the skewback and near to the left pier. As expected, significant damage develops also in the arch at the loaded span, where substantial cracks form underneath the loaded area, near to the right pier and at a location which shifts from the proximity of the right abutment towards the mid-span when the loaded area moves from l/s=0.25 to l/s=0.75.

Figure 10d shows the influence of the number of spans on the collapse load. The bridge capacity decreases significantly by increasing the number of spans from 1 to 3, while for a number of spans higher than 3 it remains practically constant. This is consistent with the fact

that at most two spans are involved in the collapse mechanism, as observed both in Figure 14 and in Figure 2.

An increase of the backfill depth to arch thickness ratio (f/d) results in an increase of the collapse load, without significant changes of stiffness (Figure 10e). The increase of collapse load is the results of the following actions of the backfill: stabilization of the arch through its own weight, spreading the loading applied at the top, opposing the deformation of the arch and the formation of cracks at the top of the arch barrel.

Figure 10f shows the influence of arch thickness to span ratio (d/s) on the stiffness and load capacity of the bridge. The different values of d/s are simulated by changing the number of rings in the masonry arches. The bridge model with the single ring arch has the same piers as the reference one, whereas the model with three-ring arches features more stocky piers. It can be observed that the stiffness and load capacity of the bridge increase significantly for increasing values of d/s. However, the observed trends are also affected by the change of pier slenderness. The collapse mechanisms observed for the case of single-ring arch and the arch with three rings are displayed respectively in Figure 15 and Figure 16.

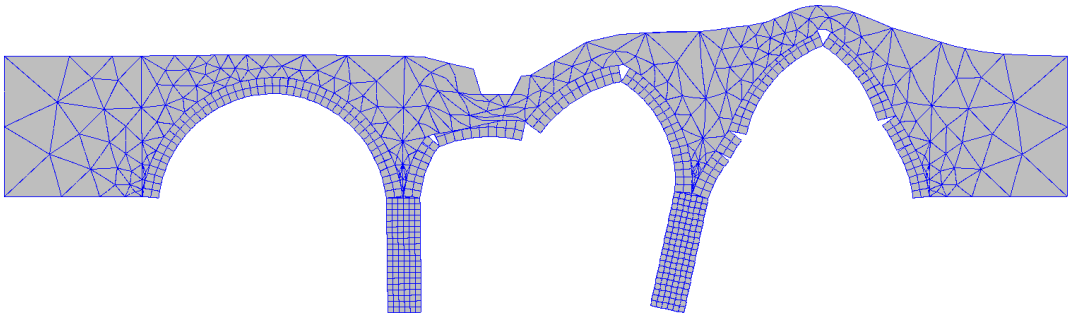
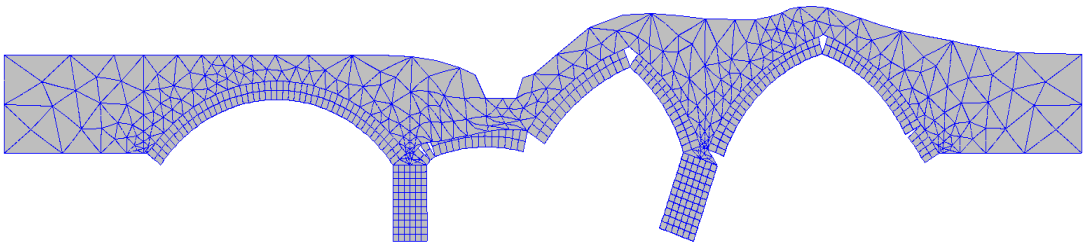


Figure 11. Collapse mechanism for rise-to-span ratio r/s=0.45.

a)



b)

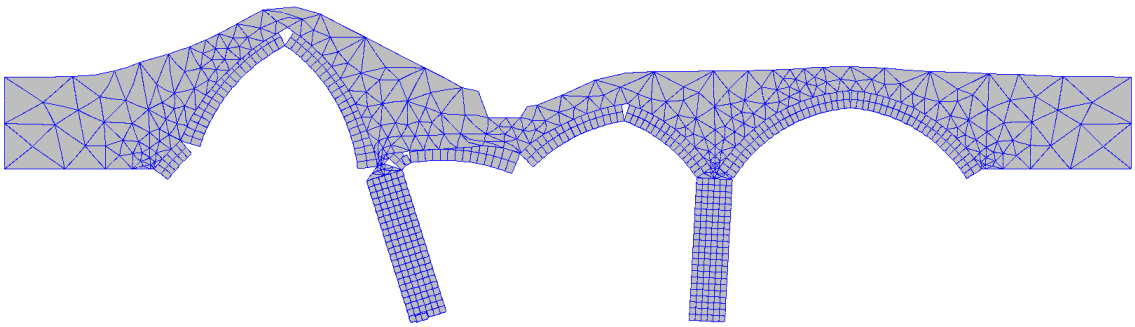
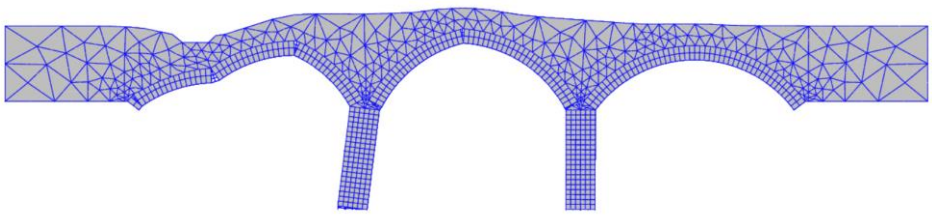
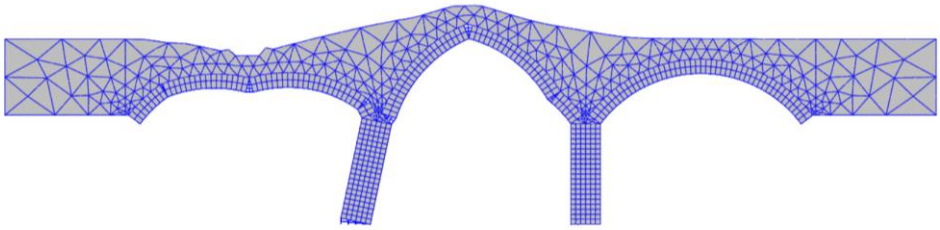


Figure 12. Collapse mechanism for pier slenderness a) h/w =2 and b) h/w=4.

a)



b)



c)

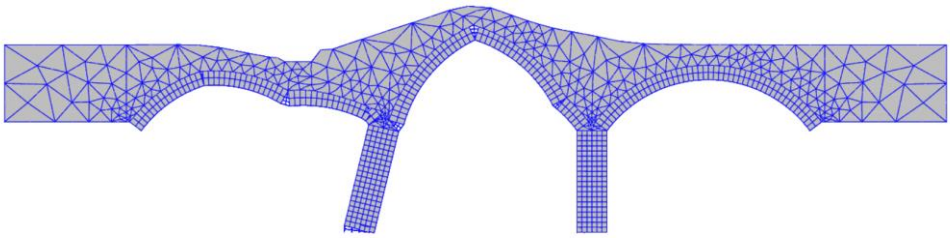
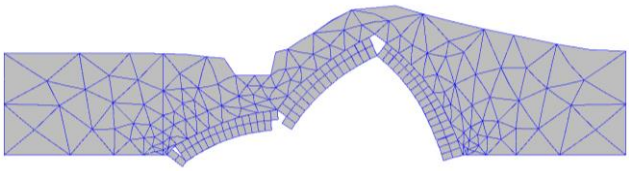
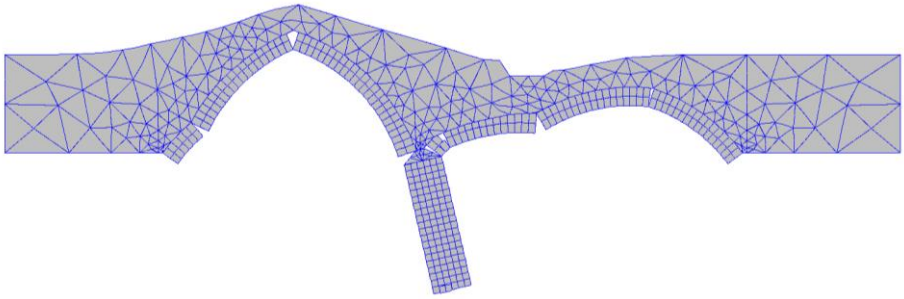


Figure 13. Collapse mechanism for different loading positions on the right-side span a) *l*/*s*=0.25, b) *l*/*s*=0.5 and c) *l*/*s*=0.75

a)



b)



c)

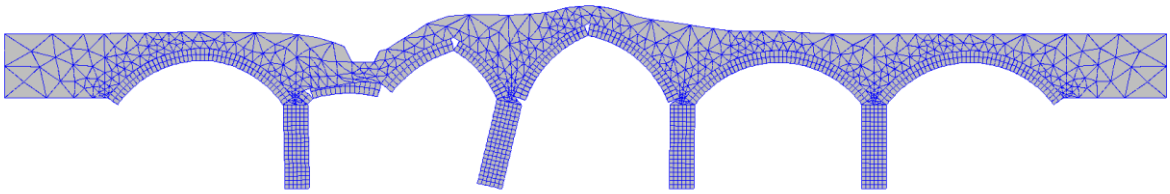


Figure 14. Collapse mechanism of: (a) one-span, (b) two-span and (c) five-span bridge.

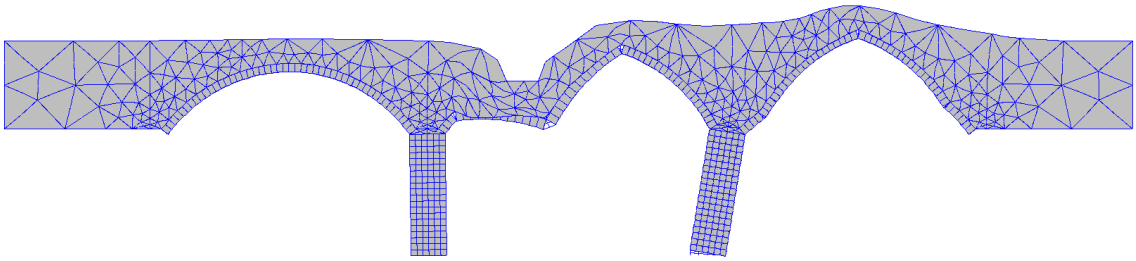


Figure 15. Collapse mechanism for arch thickness/span *d*/*s*=1/28.5 (1 ring arch).

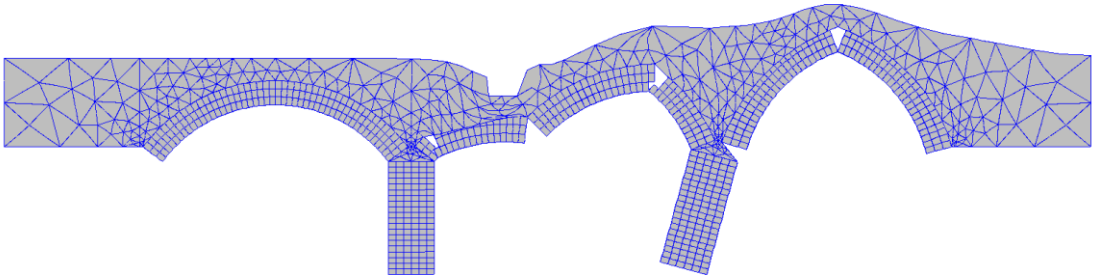


Figure 16. Collapse mechanism for arch thickness/span *d*/*s*=1/9.2 (3 rings arch).

Figure 17 summarizes the results of the investigation of the effect of the geometrical parameters on the bridge capacity. The collapse load increases with the rise-to-span ratio and reduces significantly for increasing pier slenderness values. The trend of variation with the loading position is such that the lowest resistance is found when the load is applied at the middle of the external or central span, whereas it is highest when the load is closer to the pier, as expected. The collapse load also reduces significantly by passing from the single span bridge to the three-span bridge. The resistance is practically constant for values of the fill depth to arch thickness ratio between 0 and 0.4, then it increases almost linearly for higher values. Finally, the trend of increase of the collapse load with the span is almost linear.

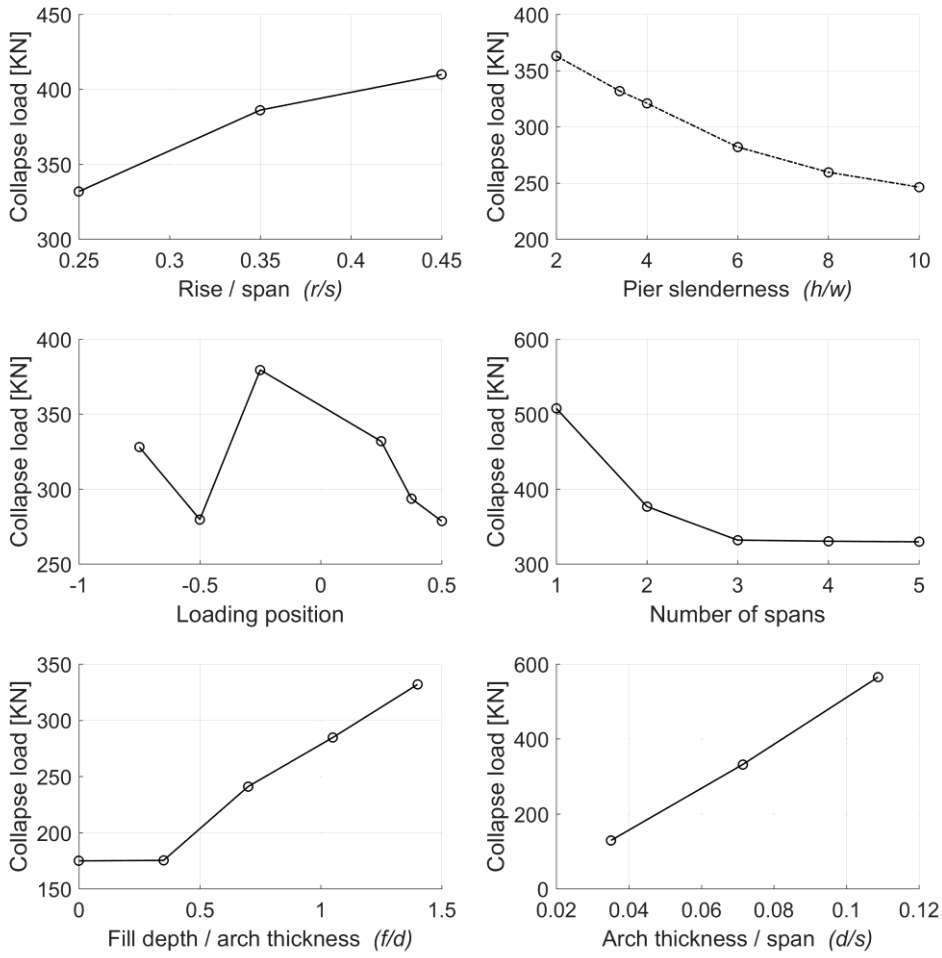


Figure 17. Influence of geometric parameters on the collapse load of the multi-span bridge.

The parametric study has been repeated for the case of the deep arch (r/s=0.45), and the most important results are summarized in Figure 18, showing the influence of the loading position, pier slenderness, number of spans, and fill depth/arch thickness on the collapse load**.** With reference to the loading position (Figure 18a), the most critical is at the midspan of the central span, as for the case of the shallow arch. The pier slenderness (Figure 18b), the number of spans (Figure 18c), and the ratio f/d have the same effect on the collapse load as for the case of the shallow arch. Higher values of the collapse loads are observed for the deep arch compared to the case of the shallow arch, for all the geometrical configurations. The average increase of the collapse load is of the order of 100 kN.

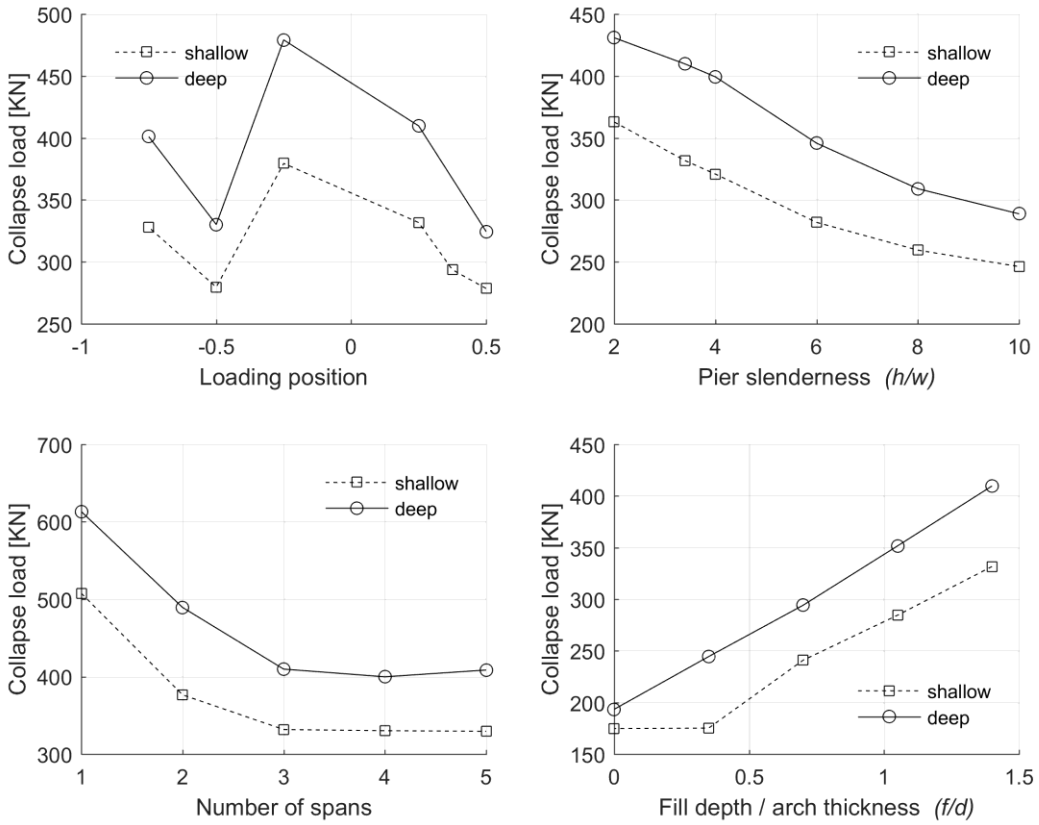


Figure 18. Influence of geometric parameters on the collapse load of the multi-span bridge with deep arch barrel.

4.3 lnfluence of mechanical parameters

This subsection shows the results of the investigation on the influence of the mechanical parameters characterising the masonry components and the backfill. In particular, Figure 19 illustrates the results related to the material parameters of the masonry constituents, namely the interface friction angle, tensile strength, and cohesion. In general, the collapse load is not very sensitive to the values assumed by these parameters. This is because the backfill contributes more significantly to the global resistance of the bridge, and this reduces the sensitivity of the collapse load to the variations of the properties of the masonry components. Similar results were observed for the case of single span masonry arch [20].

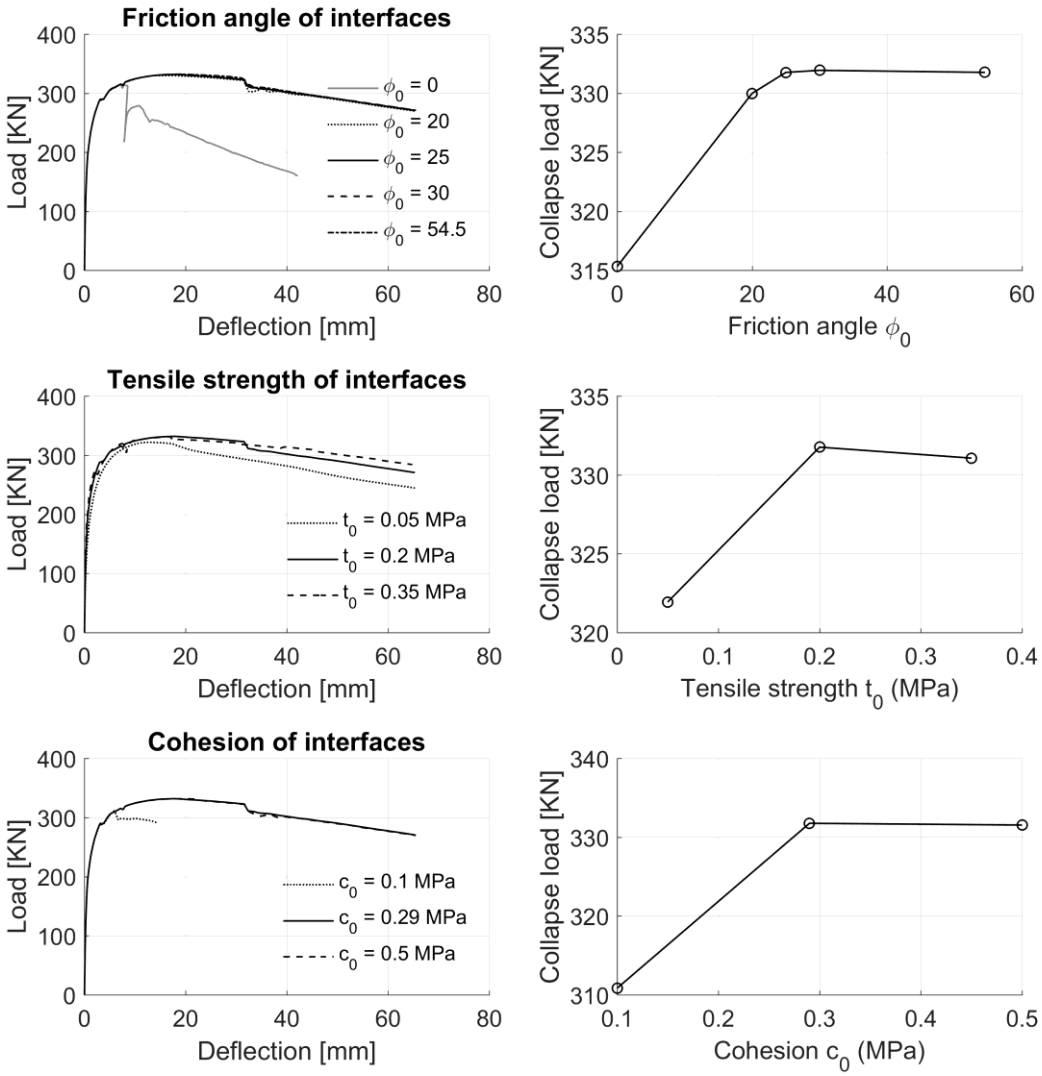


Figure 19. Influence of material properties of the arch on the global response of the reference structure.

Figure 20 illustrates the results of the analysis of the influence of the properties of the backfill material. As anticipated earlier, both the cohesion c_f and the friction angle ϕ_f of the backfill affect significant the load-carrying capacity. The backfill's Young modulus influences mainly the stiffness of the system, because at collapse the backfill experiences significant plastic deformations that are controlled by the yield surface. The bridge capacity increases from 332kN to 494kN by increasing c_f from 0.001 MPa (reference model) to 0.1MPa, whereas it increases from 301kN to 381kN by increasing ϕ_f from 45° to 65°. Increasing the Young modulus from 50MPa (reference model) to 200MPa yields an increase of the collapse load from 332kN to 370kN.

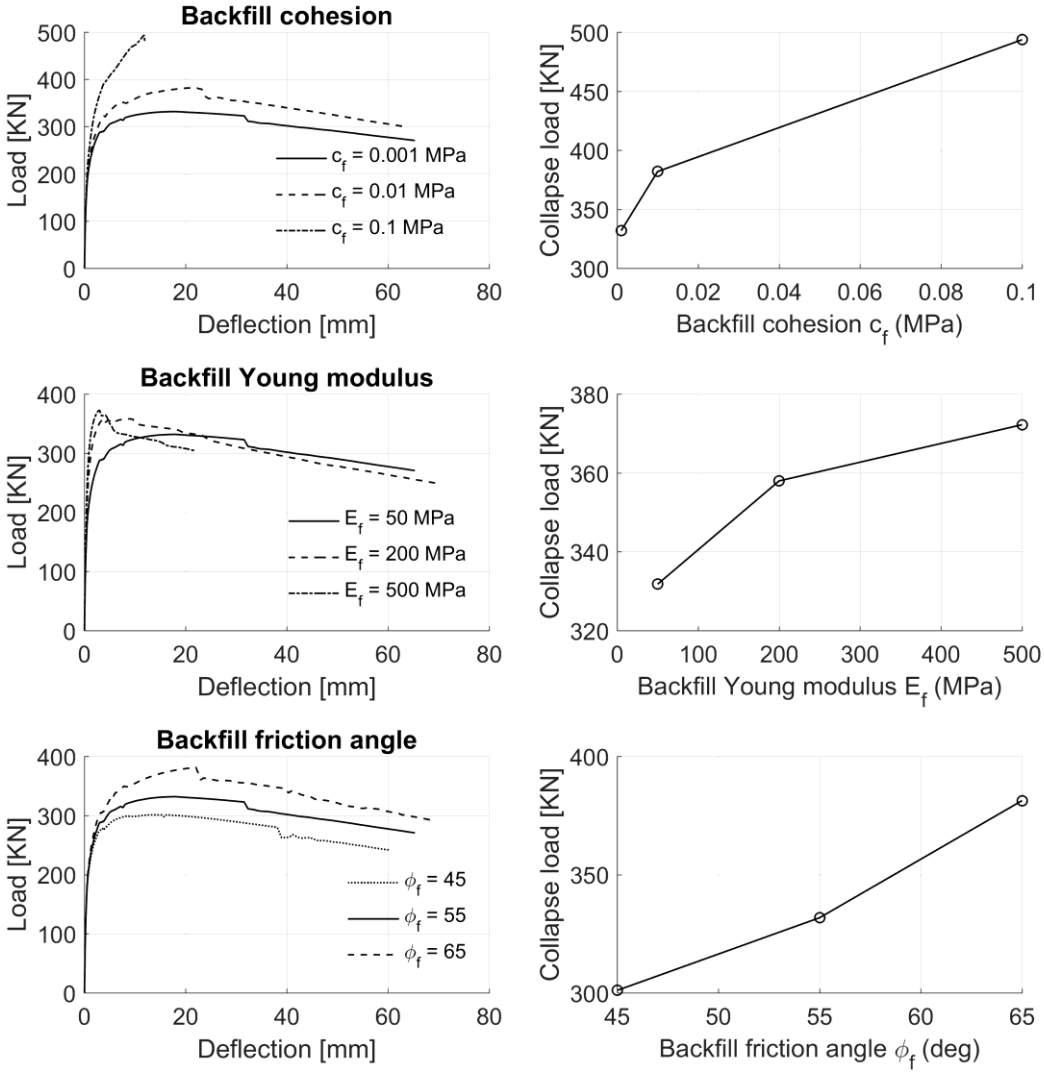


Figure 20. Influence of material properties of backfill material on the global response of the reference structure

In order to further assess how the backfill properties affect the bridge response, a new model is analysed, whose backfill is made of clay. The properties of the clay are taken from [25], and have been considered also in the case of the single span bridge analysed in [19]. The clay backfill exhibits a lower stiffness, but higher cohesion compared to the limestone backfill of the reference model. The Young modulus is taken equal to E_f=5.6 MPa, the cohesion is c_f=0.1 MPa, and the friction angle and dilatancy angle are equal φ_f=27°. While the load-deflection curves corresponding to the two different backfill materials are similar for low values of the applied displacement, they become very different for increasing displacement values up to collapse. In particular, the bridge with clay backfill exhibits a higher collapse load compared to the one with limestone backfill. Figure 21 shows the force-displacement curves for the two cases. It can be observed that the two models behave similarly only for low values of the load, whereas for higher values, the bridge with limestone fill exhibits a higher stiffness up to collapse. However, the collapse load is lower in the case of limestone fill than in the case of clay backfill. This

result is quite different from the one observed in [19], where the model with clay backfill exhibited lower stiffness and capacity.
Figure 22 shows the deformed shape of the bridge with clay backfill. The collapse mechanism differs from the one observed in the reference model (Figure 2). In fact, both the piers exhibit significant outward movements, and cracking interests all the spans. Figure 23 shows that the extent and levels of plastic deformation in the clay backfill are significantly lower than in the case of limestone backfill, with high values attained only below the loading.

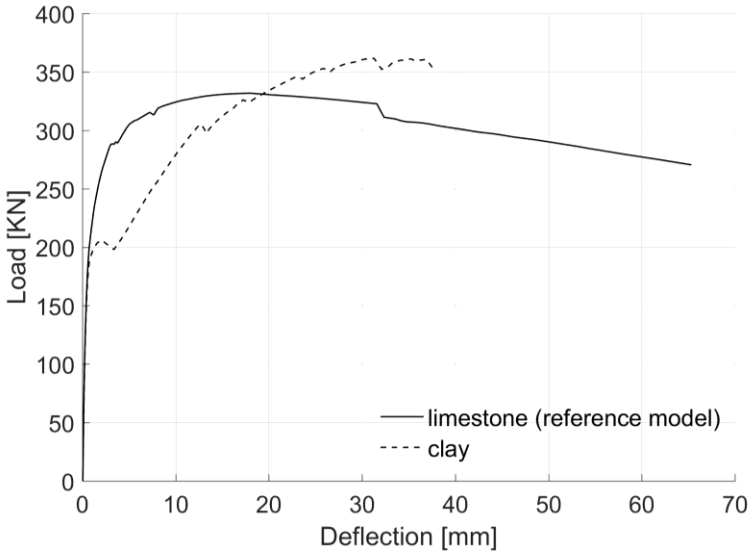


Figure 21. Influence of type of backfill material on the global response of the structure.

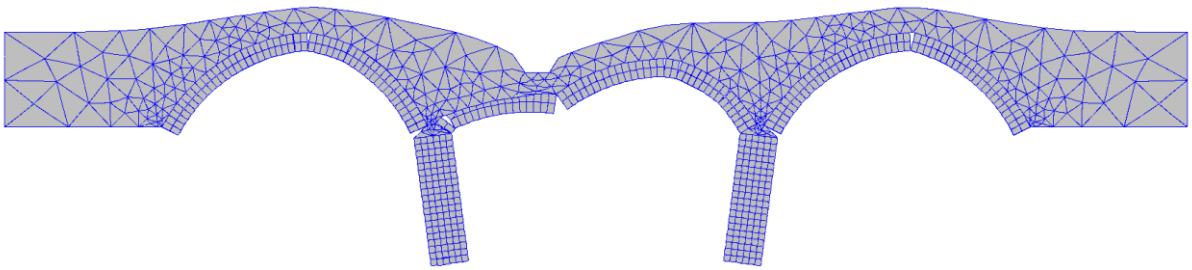


Figure 22. Deformed shape of 3-span bridge with clay backfill material corresponding to the last step of the analysis.

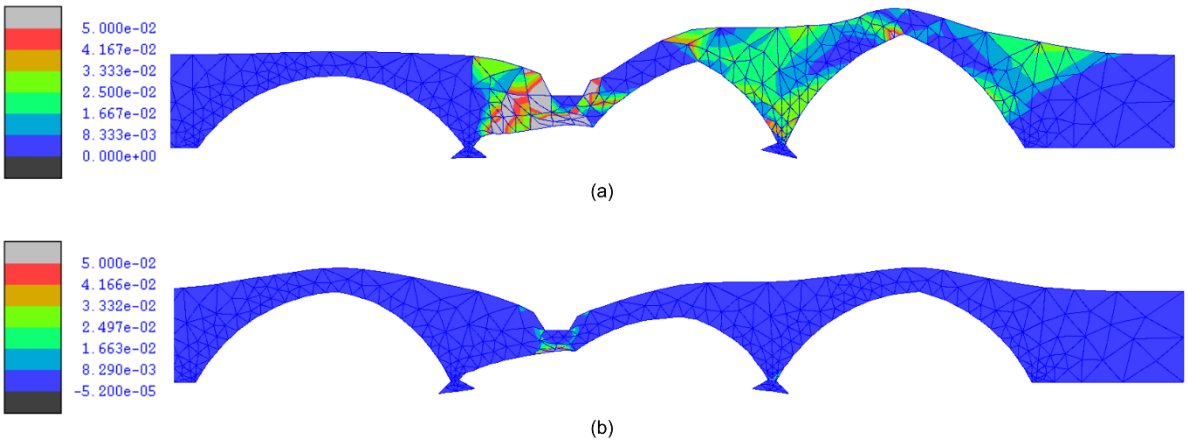


Figure 23. Plastic deformations in the backfill domain: a) limestone (reference model); b) clay.

4.4 Influence of brickwork defects

Similarly to previous works [5,19], the influence of defects in the brickwork is analysed assuming that the circumferential mortar joints connecting the two rings of the masonry arch in the reference model are degraded. The interfaces representing these weak joints are characterized by values of the initial cohesion and tensile strength 100 times smaller than those of the undamaged joints, which are reported in Table 2. Moreover, the tangent of the friction angle is assumed equal to 0.30. The deformed shape and collapse mechanism of the bridge corresponding to these weak circumferential mortar joints is shown in Figure 24. It can be observed that the collapse mechanism involves significant movement of the left pier, differently from the case of the reference bridge model whose collapse mode is characterized by a significant movement of the right one (Figure 2). Moreover, significant sliding is observed between the two rings of the central and left arches, corresponding to a dislocation of the radial mortar joints of the two rings.

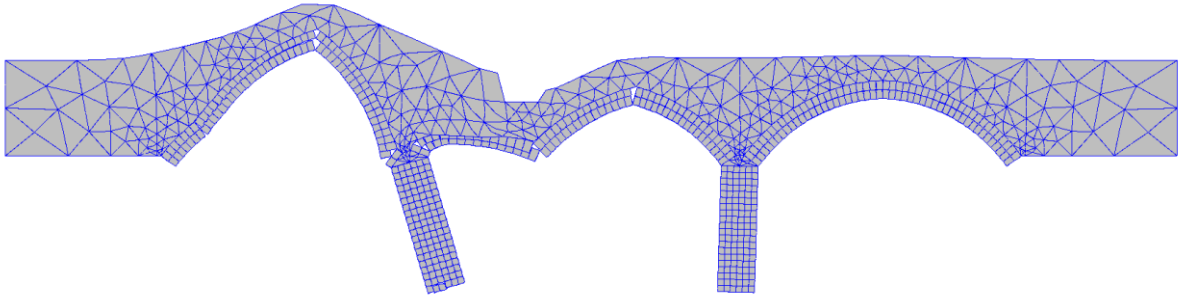


Figure 24. Collapse mechanism for of the 3-span bridge with weak circumferential mortar joints corresponding to the last step of the analysis..

Figure 25 shows the load-displacement responses obtained with the two numerical models, corresponding to damaged and undamaged circumferential mortar joints. The load capacity of the model with damaged joints (about 215 kN) is significantly lower than that of the reference model (about 330 kN). This confirms the critical influence of brickwork defects on the performance of the bridge under vertical loads.

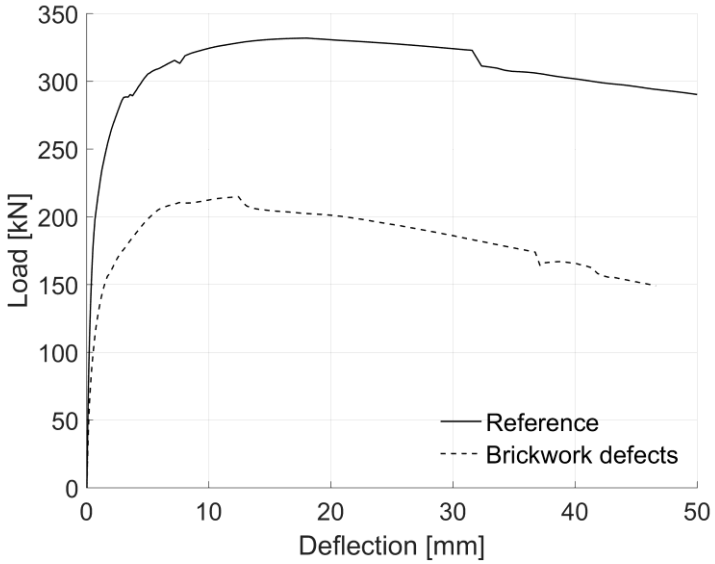


Figure 25. Influence of the weak circumferential mortar joints on the global force-displacement response of the structure.

5 CONCLUSIONS

This paper presents and discusses the results of the application of an advanced modelling approach for the analysis of multi-span masonry arch bridges. This strategy is based on the use of a mesoscale description for the masonry components, namely the arch barrels and the piers. An elasto-plastic model is used for the backfill, which interacts with the barrel through cohesive-frictional interfaces. A mortar mesh tying method to connect non-conforming meshes and a domain partitioning strategy are employed to enhance the efficiency of the computational strategy.

In the first part of the paper, the proposed modelling strategy is validated against a physical laboratory test concerning a three-span masonry arch bridge model with detached spandrel walls subjected to a vertical line load up to collapse. Subsequently, a parametric investigation is carried out to show the influence of some geometrical and mechanical parameters of the bridge on the response to vertical loads, as well as the effect of pier settlements and brickwork defects.

With regard to the influence of geometrical properties, it is found that masonry bridges with relatively shallow arch barrels are characterised by a collapse mechanism involving mainly two spans. Thus, increasing the number of spans beyond three does not change significantly the ultimate performance. On the other hand, increasing the pier slenderness results in a significant reduction of the bridge capacity, whereas increasing the rise-to-span ratio of the arch increases the collapse load. Thus, multi-span bridges with deep arch barrels exhibit higher capacity than those with shallow arch barrels. The critical loading locations leading to the lowest bridge capacities correspond to the middle of the central and the lateral spans. Moreover, the numerical results confirm that the backfill contributes crucially to the bridge response, as revealed by the fact that the bridge capacity rises remarkably by increasing the backfill depth.

With regard to the influence of mechanical properties, it is shown that the collapse load is not very sensitive to the friction angle of the interfaces, the tensile strength, and the cohesion, whereas it is very sensitive to the backfill's properties. In particular, the backfill's cohesion and friction angle have a very significant effect on the collapse load, whereas the Young modulus influences mainly the stiffness of the system.

Pier foundation settlements may influence the global stiffness of the bridge, and to a less extent the capacity, only when of significant entity. Finally, brickwork defects such as weak circumferential mortar joints result in considerable losses of the load carrying capacity in bridges with multi-ring arches.

The results of this study complement those already obtained for the case of single span bridges. Extended finite element analyses will be carried out in future research on more complex three-dimensional models capable of accounting also for the contribution of the spandrel walls on the bridge behaviour.

AKNOWLEDGEMENTS

The financial support of the European Commission through the Marie Skłodowska-Curie Individual fellowship IF ("FRAMAB", Grant Agreement 657007) for the first author is greatly acknowledged. The authors also acknowledge the Research Computing Service at Imperial College for providing and supporting the required High Performance Computing facilities.

REFERENCES

1. L. Mckibbins, C. Melbourne, N. Sawar, C. S. Gaillard, Masonry Arch Bridges: Condition Appraisal and Remedial Treatment, CIRIA, London, 2006.
2. G. Milani, P.B. Lourenço, 3D non-linear behavior of masonry arch bridges. Computers & Structures. 110-111 (2012) 133-150.
3. E Reccia, G. Milani, A. Cecchi, A. Tralli, Full 3D homogenization approach to investigate the behavior of masonry arch bridges: The Venice trans-lagoon railway bridge. Construction and Building Materials. 66 (2014) 567-586.
4. Y. Zhang, L. Macorini, B.A. Izzuddin, Mesoscale partitioned analysis of brick-masonry arches. Engineering Structures, 124 (2016) 142-166.
5. Y. Zhang, L. Macorini, B.A. Izzuddin, Numerical Investigation of Arches in Brick-Masonry Bridges, Structure and Infrastructure Engineering, 14 (2018) 14-32.
6. Y. Zhang, Advanced nonlinear analysis of masonry arch bridges. PhD Thesis, Imperial College London, UK, 2015.
7. S. Caddemi, I. Caliò, F. Cannizzaro, D. D'urso, B. Pantò, D. Rapicavoli, G. Occhipinti, 3D Discrete Macro-Modelling Approach for Masonry Arch Bridges. IABSE 2019, To-wards a resilient built environment risk and asset management, Guimaraes, Portugal.
8. V. Sarhosis, S. De Santis, G. de Felice, A review of experimental investigations and assessment methods for masonry arch bridges. Structure and Infrastructure Engineering, 12 (2016) 1439-1464.
9. Zampieri, P., Zanini, M. A., & Modena, C. (2015). Simplified seismic assessment of multi-span masonry arch bridges. Bulletin of Earthquake Engineering, 13(9), 2629-2646.
10. Scozzese, F., Ragni, L., Tubaldi, E., & Gara, F. (2019). Modal properties variation and collapse assessment of masonry arch bridges under scour action. Engineering Structures, 199, 109665.
11. T.G. Hughes, Analysis and assessment of twin-span masonry arch bridges. Proceedings of the Institution of Civil Engineers - Structures and Buildings, 110 (1995), 373-382.
12. A. Cavicchi, L. Gambarotta, Collapse analysis of masonry bridges taking into account arch–fill interaction. Engineering Structures, 27 (2005) 605-615.
13. A. Brencich, U. De Francesco, Assessment of multispan masonry arch bridges. II: Examples and applications. Journal of Bridge Engineering, 9 (2004) 591-598.
14. G. De Felice, Assessment of the load-carrying capacity of multi-span masonry arch bridges using fibre beam elements. Engineering Structures, 31 (2009) 1634-1647.
15. D.V. Oliveira, P.B. Lourenço, C. Lemos, Geometric issues and ultimate load capacity of masonry arch bridges from the northwest Iberian Peninsula. Engineering Structures, 32 (2010) 3955-3965.
16. M. Gilbert, RING Theory and modelling guide. Computational limit analysis and design unit, University of Sheffield, UK, 2005.
17. Altunışık, Ahmet C., Burcu Kanbur, and Ali F. Genc. "The effect of arch geometry on the structural behavior of masonry bridges." Smart Struct. Syst 16, no. 6 (2015): 1069-1089.

18. E. Minga, L. Macorini, B. A. Izzuddin, Enhanced mesoscale partitioned modelling of heterogeneous masonry structures. International Journal for Numerical Methods in Engineering, 113 (2017) 1950-1971.
19. Y. Zhang, E. Tubaldi, L. Macorini, B.A. Izzuddin, Mesoscale Partitioned Modelling of Masonry Bridges allowing for Arch-Backfill Interaction. Construction and Building Materials, 173 (2018) 820-842.
20. E. Tubaldi, L. Macorini, B.A. Izzuddin, Identification of critical mechanical parameters for advanced analysis of masonry arch bridges, Structure and Infrastructure Engineering, 16, 2 (2020) 328–345.
21. E. Tubaldi, L. Macorini, B.A. Izzuddin, Three-dimensional mesoscale modelling of multi-span masonry arch bridges subjected to scour. Engineering Structures, 165 (2018), 486-500.
22. E. Tubaldi, L. Macorini, B.A. Izzuddin, Nonlinear mesoscale analysis of multi-span masonry bridges, The Tenth International Masonry Conference, Milano (Italy), 2018, 411-423.
23. C. Melbourne, M. Gilbert, M. Wagstaff, The collapse behaviour of multispan brickwork arch bridges. The Structural Engineer, 75 (1997), 297-305.
24. A.W. Page, The biaxial compressive strength of brick masonry. Proceedings of the Institution of Civil Engineers, 71 (1981) 893-906.
25. P.J. Fanning, T.E. Boothby, B.J. Roberts, Longitudinal and transverse effects in masonry arch assessment. Construction and Building Materials, 15 (2001) 51-60.
26. L. Macorini, B.A. Izzuddin, A non-linear interface element for 3D mesoscale analysis of brick-masonry structures. International Journal for Numerical Methods in Engineering, 85 (2011) 1584-1608.
27. E. Minga, L. Macorini, B.A. Izzuddin, A 3D mesoscale damage-plasticity approach for masonry structures under cyclic loading. Meccanica, 53 (2018) 1591–1611.
28. S. Dolarevic, A. Ibrahimbegovic, A modified three-surface elasto-plastic cap model and its numerical implementation, Computers & Structures, 85 (2007) 419-430.
29. E.A. De Souza Neto, D. Peric, D.R.J. Owen, Computational Methods for Plasticity: Theory and Applications, Wiley, 2008.
30. G.A. Jokhio, Mixed dimensional hierarchic partitioned analysis of nonlinear structural systems, PhD Thesis, Imperial College London, UK, 2012.
31. G.A. Jokhio, B.A. Izzuddin, Parallelisation of nonlinear structural analysis using dual partition super elements, Advances in Engineering Software, 60 (2013) 81-88.
32. G.A. Jokhio, B.A. Izzuddin, A dual super-element domain decomposition approach for parallel nonlinear finite element analysis, International Journal for Computational Methods in Engineering Science and Mechanics, 16 (2015) 188-212.
33. B.A Izzuddin, Nonlinear dynamic analysis of framed structures, PhD Thesis, Imperial College, London, UK, 1991.
34. G.N. Pande, J.X. Liang, J. Middleton, Equivalent elastic moduli for brick masonry, Computers and Geotechnics, 8 (1989), 243-265.

35. C. Melbourne, M. Gilbert, The behaviour of multiring brickwork arch bridges, Structural Engineer, 73, 1995.
36. A. Brencich, R. Morbiducci, Masonry Arches: Historical Rules and Modern Mechanics, International Journal of Architectural Heritage, 1 (2007) 165-189.
37. S. De Santis, G. De Felice, Overview of railway masonry bridges with a safety factor estimate. International Journal of Architectural Heritage, 8 (2014), 452-474.
38. Zampieri, P., Zanini, M. A., Faleschini, F., Hofer, L., Simoncello, N., & Pellegrino, C. Structural assessment of masonry arch bridges with settled supports. IABSE Symposium 2019 Guimaraes Towards a Resilient Built Environment - Risk and Asset Management March 27-29, 2019, Guimaraes, Portugal.